

Dec.2023 / Vol.184

M i t s u b i s h i E l e c t r i c

ADVANCE

High Frequency & Optical Devices

• **Editorial-Chief**

Masahiro Otani

• **Editorial Advisors**

Kenichiro Kurahashi

Hisao Takahashi

Omi Kuriwaki

Asuka Omori

Hiroyuki Teranishi

Satoshi Watanabe

Kenichi Uto

Tsutomu Matsubara

Yasumasa Yamanaga

Takao Ikai

Kunihiko Egawa

Hideya Tadokoro

Kenji Okuma

Yusuke Hirata

Satoru Yamaguchi

Yoshihiro Yamaguchi

Kohei Miki

• **Vol. 184 Feature Articles Editor**

Yoshihisa Tashiro

• **Editorial Inquiries**

Masahiro Otani

Corporate Productivity Engineering &
Logistics Dept.

Fax: +81-3-3218-2465

Mitsubishi Electric Advance is published on line quarterly (in March, June, September, and December) by Mitsubishi Electric Corporation. Copyright © 2023 by Mitsubishi Electric Corporation; all rights reserved. Printed in Japan.

The company names and product names described herein are the trademarks or registered trademarks of the respective companies.

CONTENTS

Overview 1
by *Kenji Masuda*

Technical Reports

10W Class, Wideband GaN Power Amplifier Module for 5G Base – Stations 2
by *Shuichi Sakata and Marie Taguchi*

Wider – temperature – range CWDM 100Gbps EML Chip for Data Centers 7
by *Yusuke Azuma and Akitsugu Niwa*

50Gbps DFB Laser Diode for 5G Base Stations 10
by *Go Sakaino and Masaaki Shimada*

1.55µm Tunable DFB-LD for 400G Digital Coherent Optical Transmission System 13
by *Kazuki Yamaji and Ryosuke Nagao*

Thermal Diode Infrared Sensor “MeDIR” and User Support Tools 16
by *Yasuki Aihara and Satoshi Okuda*

Precis

Digital transformation (DX) advances innovation in business activities and transformation in lifestyles, so the importance of communications infrastructure and sensor technology is rising. In this issue, we introduce highly efficient GaN amplifiers and high-speed optical devices for the latest information communications, as well as infrared sensor modules required in applications in the areas of crime prevention and surveillance.

Overview



Author: *Kenji Masuda**

The Latest Status and Future Outlook of High Frequency & Optical Devices

Due to the progress in digital transformation (DX) that is revolutionizing products, services, and business models through the utilization of data and digital technology, innovation in business activities and a shift to new lifestyles are advancing on a global scale. Consequently, information communication infrastructure to support DX is becoming increasingly important. Accompanying the preparation of communication infrastructure and data centers with larger capacities, achieving low power consumption as well as high speeds in the high frequency and optical devices essential to the infrastructure is a significant development issue.

5th generation mobile communication system (5G) features Enhanced Mobile Broadband (eMBB), Ultra Reliable and Low Latency Communications (URLLC) and Massive Machine Type Communications (mMTC), uses array antennae with several antenna elements arranged in the base stations, and is able to simultaneously and efficiently send wideband, modulating signals to each user terminal. For electric power amplifiers for use in 5G base stations, in addition to the establishment of both highly efficient and highly linear operations, there is an increasing demand for wideband operations. For this use, Mitsubishi Electric is developing and productizing a compact, highly efficient, wideband gallium nitride (GaN) amplifier that generates little heat.

Meanwhile, in optical communication networks which are a core part of the communication infrastructure, we are increasing the speed and the transmission capacity of all network layers including in data centers. We are developing optical devices capable of multi-value modulation which doubles the transmission signal capacity per unit time, to realize the low power consumption products of the Distributed FeedBack Laser (DFB-LD) at 50 Gbps and the Electro-absorption Modulated Laser (EML) at 100 Gbps.

Furthermore, we are progressing with the implementation of a high pixel count and the expansion of the detection temperature range for the high-performance, compact, low-cost infrared sensor module, "MeIDIR." We hope to apply this in a wide range of fields such as in-vehicle monitoring in addition to uses like crime prevention, indoor monitoring, people counting, and smart buildings.

* Senior General Manager, High Frequency & Optical Device Works

10W Class, Wideband GaN Power Amplifier Module for 5G Base – Stations

Authors: *Shuichi Sakata** and *Marie Taguchi**

1. Introduction

In recent years, implementation of 5th generation mobile communication system (5G) has spread to meet the demand for high speed, large capacity communications. If a single amplifier module is able to support a variety of frequencies, then this contributes to low cost and joint use of the radio units of 5G base stations. In this article, we discuss the 10W class, wideband GaN power amplifier module for 5G base stations which covers almost all the bandwidths of 5G frequencies in the 3 - 4 GHz band.

2. Background

In recent years, implementation of 5G has spread to meet the demand for high speed, large capacity communications. The 5G frequencies allocated in the 3 - 4 GHz band are distributed across a frequency range of the order of 700 MHz depending on the country or region. When using a conventional amplifier module, the operating bandwidth is at most of the order of 400 MHz, so it was difficult to cover all the 5G frequencies in the 3 - 4 GHz band with a single amplifier. If a single amplifier module is able to support a variety of frequencies, then this contributes to low cost and joint use of the radio units of 5G base stations. The Doherty power amplifier, which has been used until now for the amplifier module's final stage, has a narrow band, so extending it to wideband use was difficult. In addition, the design method⁽¹⁾ which configures the load modulation circuit in the Doherty power amplifier using the Tee-Type network in the Doherty power amplifier's main amplifier, proposed as a method to realize compact, highly efficient wideband from before, and using the transistor's parasitic capacitance without placing a circuit in the auxiliary amplifier, was difficult to employ in this module's configuration because a circuit has to be placed in the auxiliary amplifier.

In this article, we will discuss a new design method which realizes wider band operations even when a circuit is placed in the auxiliary amplifier, while making use of the advantages of the conventional design method, by designing the main amplifier and auxiliary amplifier circuit in an integrated manner. Using this design method, we created and evaluated a prototype 10W class, GaN power amplifier module with the result that, in the 700 MHz band from 3.4 - 4.1 GHz, the Adjacent Channel

Leakage Ratio (ACLR) after digital pre-distortion was -46 dBc with a 20 MHz modulation bandwidth signal, while a Power Added Efficiency (PAE) of 42.0 - 44.6% and a gain of 28.6 - 31.0 dB were achieved.

3. Doherty Power Amplifier's New Circuit Design Method

The circuit diagram of the Doherty power amplifier designed is shown in Fig. 1. The main amplifier and the auxiliary amplifier are represented ideally with the current source and the shunt parasitic capacitance ($C_{ds,m}$, $C_{ds,a}$). We place the Tee-Type network composed of the transmission line between the main amplifier and the combining point, and set their electrical lengths and characteristic impedances to θ_1 , θ_2 , θ_3 , Z_1 , Z_2 , Z_3 respectively. We place the Tee-Type network composed of the lumped component between the auxiliary amplifier and the combining point, and it is composed of the series inductor L_{a1} , the shunt inductor L_{a2} , and the series capacitor C_{a1} respectively. The series inductor L_{a1} is assumed to be a wire to the transistor. When there is a multi-chip configuration like a module, because it is necessary to connect the external circuit to the transistor with a wire, a circuit must be placed in-between the auxiliary amplifier and the combining point.

Next, we will discuss the circuit's operation principle. The circuit design method proposed in this article differs from conventional circuit design methods in that it transforms the impedance at the combining point. Specifically, as shown in Fig. 1, the impedance viewed at the output from the combining point is transformed into $\gamma \cdot (R_{opt,m} // R_{opt,a})$ and $\gamma = 1$ for conventional circuit designs, but in this circuit design method, it is possible to set $\gamma > 1$ because the circuit is inserted into the auxiliary amplifier side. Here, the γ represents the impedance transformation ratio, and $R_{opt,m}$, $R_{opt,a}$ represent the main amplifier's and the auxiliary amplifier's optimal impedances respectively. To operate as a Doherty power amplifier, both the main amplifier and the auxiliary amplifier are required to match the optimal impedances ($R_{opt,m}$, $R_{opt,a}$) respectively at saturation. In the case of this circuit, as shown in Fig. 1(b), it is easy to understand the operation if the circuit is replaced by an equivalent circuit that adds the virtual shunt capacitor (C_{vir}) and the virtual shunt inductor (L_{vir}) which cancel each other

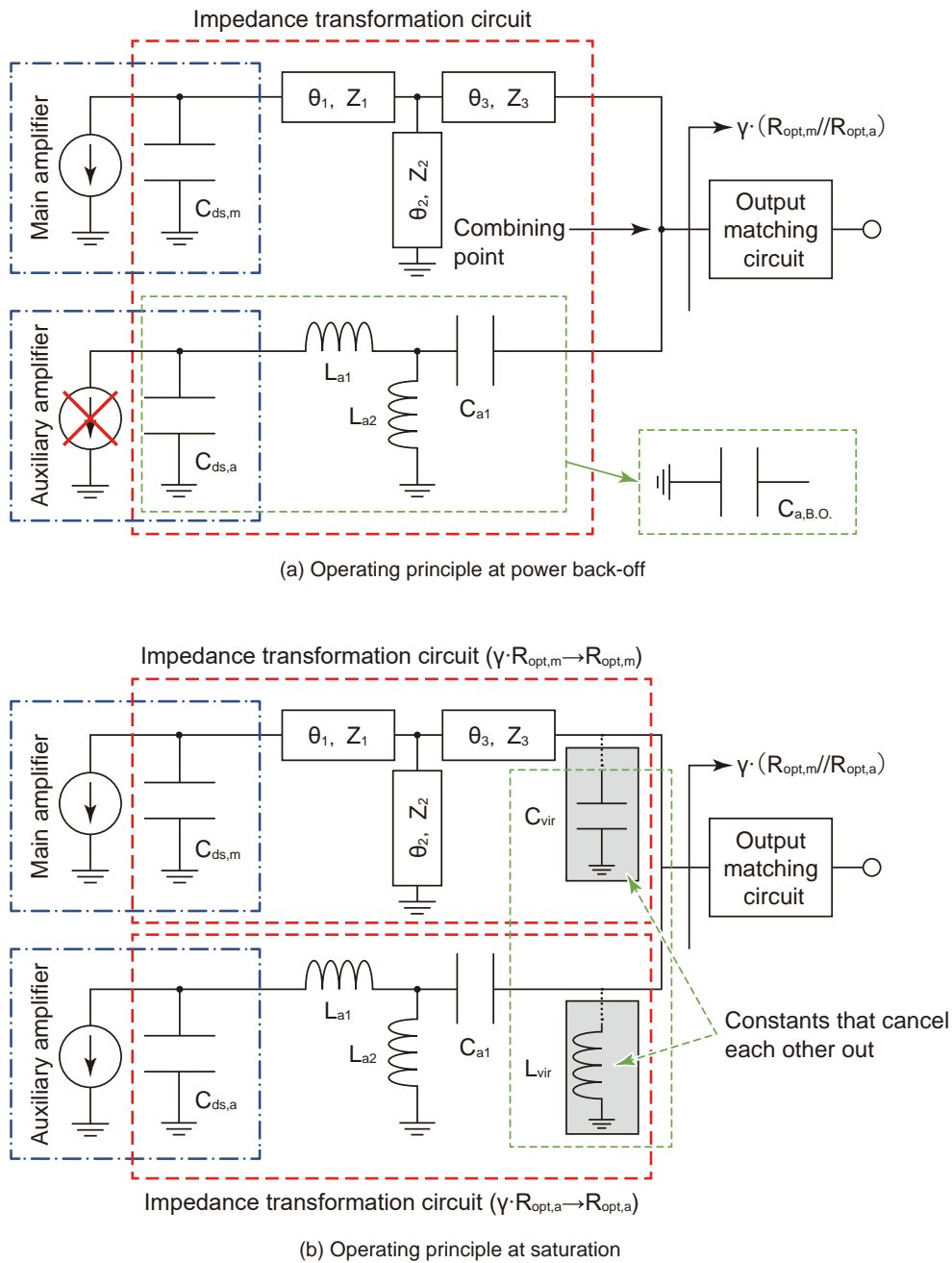


Fig. 1 Circuit schematics of designed Doherty power amplifier

out at the combining point. These virtual components together form an impedance transformation circuit that provides the impedance transformation ratio γ for both the main amplifier and the auxiliary amplifier. While at power back-off, to function as a Doherty power amplifier, the combining circuit must function as a load modulation circuit for the main amplifier. As shown in Fig. 1(a), at power back-off, the auxiliary amplifier has halted operation, so the current source on the auxiliary amplifier side is open. At this time, the four elements of

the auxiliary amplifier side circuit, $C_{ds,a}$, L_{a1} , L_{a2} , and C_{a1} , can be represented equivalently as a shunt capacitor ($C_{a,B.O.}$). This equivalent shunt capacitor ($C_{a,B.O.}$) and the main amplifier's Tee-Type network can form the load modulation circuit in the Doherty power amplifier with the main amplifier side parasitic capacitance ($C_{ds,m}$). In this way, it is possible to function as a Doherty power amplifier through this circuit, however, it is not easy to find circuit constants to satisfy these operating conditions at saturation and at power back-off. Therefore, we

established a circuit equation to satisfy the conditions shown in Fig. 1. In this case, when the values of Z_1 , Z_2 , Z_3 , L_{a1} , γ , C_{vir} in the circuit are fixed, the other circuit parameters (θ_1 , θ_2 , θ_3 , L_{a2} , C_{a1}) can be analytically determined uniquely. Therefore, as the parameters of the Z_1 , Z_2 , Z_3 , and L_{a1} are determined by the module structure, at the circuit design stage when the module structure has been decided, it is not possible to choose them arbitrarily. Therefore, γ , C_{vir} can be arbitrarily chosen at the circuit design stage. However, not all combinations of γ , C_{vir} have solutions for which the circuit operates as a Doherty power amplifier, and indeed we have found out from circuit analysis that combinations that have solutions are limited. Furthermore, we have discovered that, among the combinations for which there are solutions, the solutions in which γ is made large are consistent with wideband. In Fig. 2, we show the results of simulating the frequency dependence of the Doherty power amplifier's load modulation using the current source model. In

Fig. 2(a) and (b), the main amplifier side impedance (Γ_{main} , $\Gamma_{main(B.O.)}$) and the auxiliary amplifier side impedance (Γ_{aux}) are shown in a Smith Chart normalized to their respective optimal impedances. Regarding the main amplifier side impedance, the impedance loci of the respective frequencies are shown in a thin, solid line, and the frequency dependence of the impedance at power back-off are shown in a thick, solid line. In Fig. 2(c) and (d), the frequency dependence of the magnitude of the reflection coefficients corresponding to the respective optimal impedances are shown at saturation (thin, solid line) and at power back-off (thick, solid line) for the main amplifier, and only at saturation (dotted line) for the auxiliary amplifier. The parameters used in this simulation other than γ as follows.

$$Z_1=Z_2=Z_3=R_{opt,m}, C_{vir}=0.9 \cdot C_{ds,m}$$

From the diagram, we can see that wider band matching is obtained when $\gamma = 1.8$. In particular, we can see that a wideband characteristic is obtained for

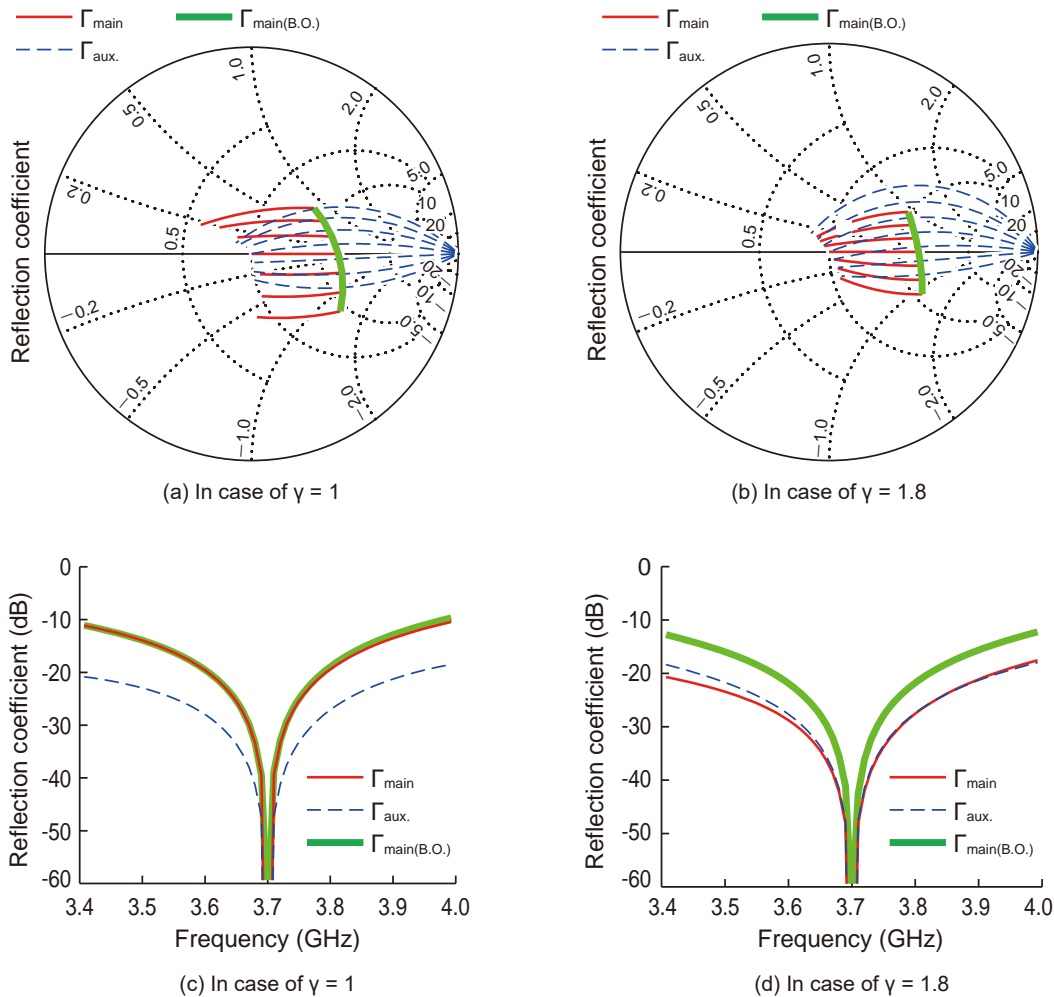


Fig. 2 Simulation result of frequency dependence of impedance modulation in Doherty Power Amplifier using current source model

the main amplifier's impedance at saturation. Based on this we see that a wider band Doherty power amplifier operation is possible than conventionally ($\gamma = 1.0$) due to this circuit design method.

4. Results of Creation and Evaluation of a Prototype 10W Class, Wideband GaN Power Amplifier Module for 5G Base Stations

We conducted design and prototype creation of the 10W class, wideband GaN power amplifier module for 5G base stations that in the final stage had a Doherty power amplifier that used the circuit design method of Chapter 2. Figure 3 shows the module that was designed and prototyped. The module's effective area is 76 mm². Figure 4 shows the results of the evaluation when a 3.9 GHz pulse modulated signal was used. The graph's vertical axis indicates the final stage Doherty power amplifier's drain efficiency (DE (final)), the PAE including the driver stage's power consumption, and the Gain; and the horizontal axis indicates the output power (Pout). From the diagram we see that for the designed and prototyped module, at the peak output power of 47.9 dBm and 8 dB power back-off point, the drain efficiency is 53.8%, the PAE is 45.7%, and the Gain is 31.7 dB. Figure 5 shows the frequency dependence of the results of the evaluation using the modulation signal that has a 20 MHz modulation bandwidth and a 7.5 dB Peak to Average Power Ratio (PAPR). In the evaluation, the Digital Pre-Distortion (DPD) is applied and the post-DPD characteristics are represented. From the diagram we see that smooth characteristics are obtained across the 700 MHz from 3.4 - 4.1 GHz. In the 700 MHz band, the characteristics obtained are: average output power (Pave) of 40.3 - 40.8 dBm, PAE of 42.0 - 44.6%, Gain of 28.6 - 31.0 dB, post-DPD ACLR of less than -46 dBc. Figure 6 shows the results of the DPD evaluation using the 5G NR (New Radio) 100 MHz modulation signal. As shown in the diagram, we were able to apply DPD even for a wideband modulation signal, and we were able to obtain a characteristic of -51,7 dBc for the post-DPD ACLR. Table 1 shows the comparison between the amplifier with the design described in this article and other amplifiers for 3 - 4 GHz. We see that this designed and prototyped amplifier module shows the widest bandwidth characteristics in the 3 - 4 GHz band. From this conclusion, we were able to demonstrate the effectiveness of this design method.

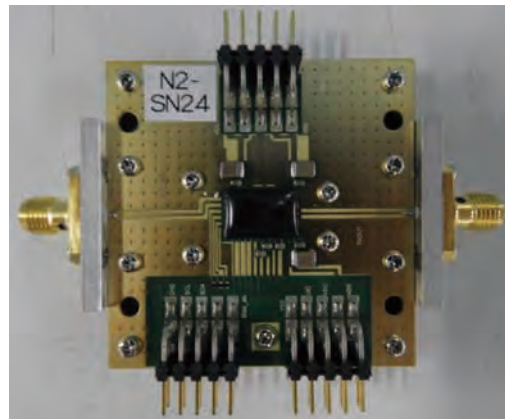


Fig. 3 Designed and fabricated 10W Class, Wideband GaN Power Amplifier Module for 5G Base-Stations

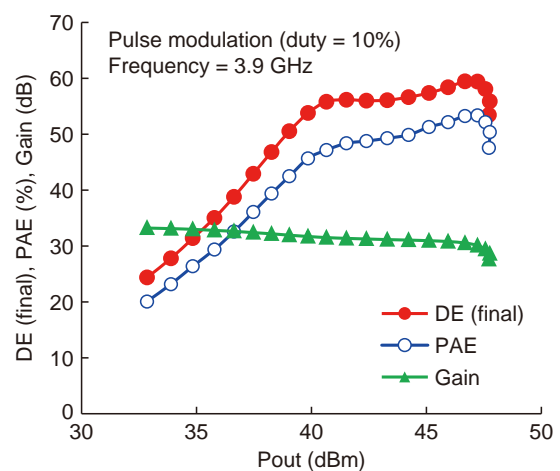


Fig. 4 Measurement result of fabricated power amplifier module using pulse modulated signal at 3.9 GHz

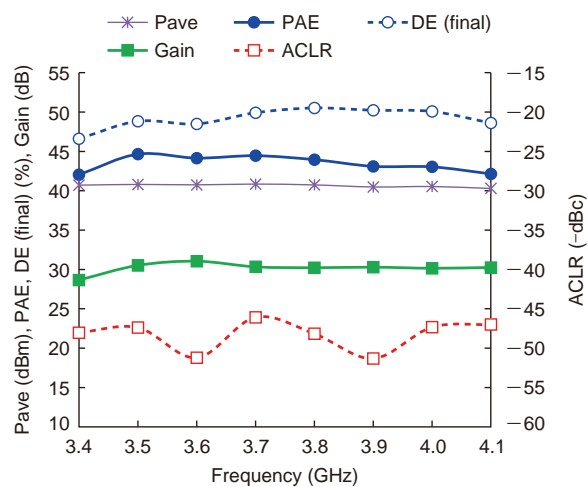


Fig. 5 Measured frequency characteristic using 20 MHz modulation signal with 7.5 dB PAPR

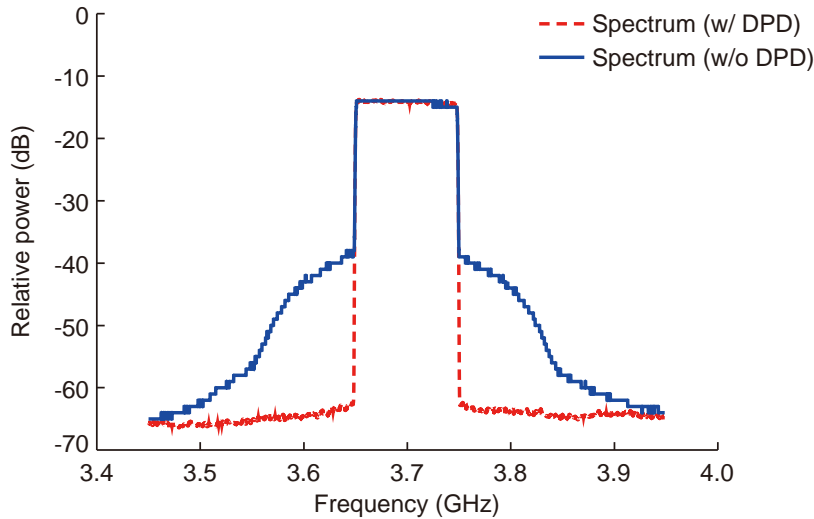


Fig. 6 Measured spectrum of the output signal using 5G NR 100MHz modulation signal before and after DPD

Table 1 Comparison of the designed power amplifier module with other amplifier operating in 3-4 GHz band

| Amplifier | Frequency (GHz) | Drain efficiency (%) | PAE (%) | Modulation bandwidth (MHz) | PAPR (dB) |
|---------------------|-----------------|----------------------|-----------|----------------------------|-----------|
| References (2) | 3.3-3.6 | | 40 | 20 | 7.2 |
| References (3) | 3.4-3.8 | 50.4-54.8 | 42.9-47.8 | 20 | 8 |
| References (4) | 3.0-3.6 | 45.9-50.2 | | 20 | 7.5 |
| Developed this time | 3.4-4.1 | 46.6-50.5 | 42.0-44.6 | 20 | 7.5 |

5. Conclusion

We have described a new design method which, because it covers almost all the 5G frequencies in the 3 - 4 GHz band, realizes a wider band operation while making use of the advantages of the conventional design method. As a result of using this design method to prototype and evaluate a 10W class GaN amplifier module, in the 700 MHz band from 3.4 - 4.1 GHz, an ACLR after digital pre-distortion of -46 dBc was satisfied with a 20 MHz modulation bandwidth signal, and a PAE of 42.0 - 44.6% and a gain of 28.6 - 31.0 dB were achieved. In addition, from the fact that the widest bandwidth characteristics were obtained compared to other amplifiers, we were able to demonstrate the effectiveness of this design method.

References

- (1) Gustafsson, D., et al.: A wideband and compact GaN MMIC Doherty amplifier for microwave link applications, IEEE Transactions on Microwave Theory and Techniques (2013)
- (2) Maroldt, S., et al.: 3.5-GHz ultra-compact GaN class-E integrated Doherty MMIC PA for 5G massive MIMO base station applications, European Microwave Integrated Circuits Conference (2017)
- (3) Sakata, S., et al.: A fully integrated GaN Doherty power amplifier module with a compact frequency-dependent compensation circuit for 5G massive MIMO base stations, IEEE/MTT-S International Microwave Symposium (2020)
- (4) Komatsuzaki, Y., et al.: 3.0 - 3.6 GHz wideband, over 46% average efficiency GaN Doherty power amplifier with frequency dependency compensating circuits, IEEE Topical Conference on RF/Microwave Power Amplifiers for Radio and Wireless Applications (2017)

Wider - temperature - range CWDM 100Gbps EML Chip for Data Centers

Authors: Yusuke Azuma* and Akitsugu Niwa*

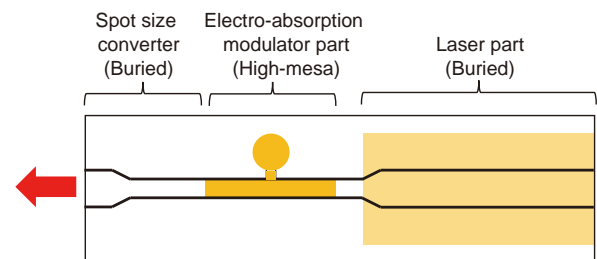
1. Introduction

Along with the rapid increase in data communication capacity, data center network communication speeds and capacities continue to increase. Meanwhile, because power consumption is expanding greatly since many transmission devices are being driven and cooled, the demand for low power consumption is extremely strong. Furthermore, reducing the cost of transmission equipment is also extremely important. To handle these issues, using an Electro-absorption Modulated Laser (EML) that does not require temperature adjustment and operates at a wide range of temperatures is effective. A method to realize 400 Gbps data communication using a four-wavelength EML chip operating at 100 Gbps is enacted in an Multi Source Agreement (MSA)⁽¹⁾. The four wavelengths use a Coarse Wavelength Division Multiplexing (CWDM) standard in which the wavelength interval is 20 nm and each wavelength allowable width is 13 nm. Until now, Mitsubishi Electric has developed a single wavelength 50 Gbps EML with a chip temperature range of 25 - 75°C which operates without the need for temperature adjustment, but some data centers are now deemed to require an EML chip which operates at a wider temperature range of $T_{LD} = 5 - 85^{\circ}\text{C}$ with no temperature adjustment. In addition, for 400 Gbps transmission, operation of 100 Gbps per wavelength is required. We developed a semiconductor laser diode chip which is applied as a light source in optical transceivers for 400 Gbps optical fiber communication in data centers. 100 Gbps operation is available in temperatures ranging from 5 to 85°C due to optimized design parameters for the laser diode and modulator sections.

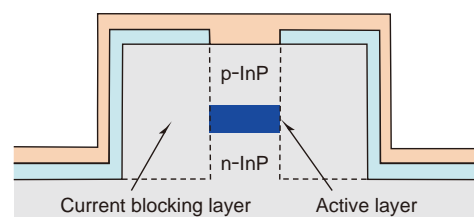
2. EML Chip Design

Figure 1 shows the EML device structure. For the laser part, we used a buried heterostructure (Fig. 1(b)) with excellent high temperature characteristics. For the electro-absorption modulator, we decided on a high mesa structure (Fig. 1(c)) possessing high extinction ratio and wide bandwidth characteristics, and the entire device employed our proprietary hybrid waveguide structure which integrated them monolithically (Fig. 1(a))⁽²⁾. For the 100 Gbps high speed operation here, it is necessary to secure both wide bandwidth and extinction ratio through the reduced capacity of the Electro-Absorption Modulator (EAM). To reduce the capacity and obtain a wide bandwidth,

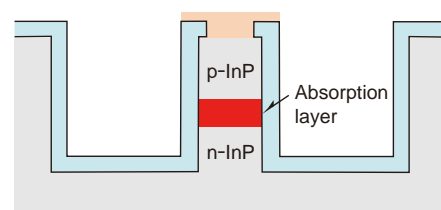
it is desirable to shorten the length of the electro-absorption modulator, but there is a trade-off whereby if the electro-absorption modulator is shortened, the extinction ratio is reduced. The high mesa structure can increase the ratio of optical confinement in the Electro-Absorption (EA) layer compared to other ridge types or buried structures, so it is possible to obtain a high extinction ratio even with a short modulator length. For that reason, here we employed the high mesa structure which can ease the trade-off between the bandwidth and the extinction ratio. The electro-absorption modulator length was made even shorter than the conventional devices and the capacity was reduced, but the design of the extinction ratio that is part of the trade-off satisfied the FR4 standard⁽¹⁾ of the 100 G Lambda MSA. In addition, the fiber coupling efficiency of the single mode fiber was increased by installing a spot size converter following the EAM.



(a) Top view of entire chip



(b) Cross-sectional view of buried LD



(c) Cross-sectional view of high-mesa EAM

Fig. 1 Schematic structure of hybrid-waveguide EML

Normally, the absorption layer is formed by a multiple quantum well. Turning the light on and off is controlled using a phenomenon (quantum confined stark effect) in which the light's absorption spectrum shifts to the long wavelength side due to the application of an electric field across the quantum well. As in Fig. 2, light from the laser part which is incident on the Electro-Absorption layer passes through when there is no electric field, but when an electric field is applied, the band gap narrows to allow light to be absorbed. Figure 3 shows an overview of the electro-absorption modulator's absorption spectrum. In the absence of an electric field, the absorption coefficient of the laser oscillator wavelength is small and so the light passes

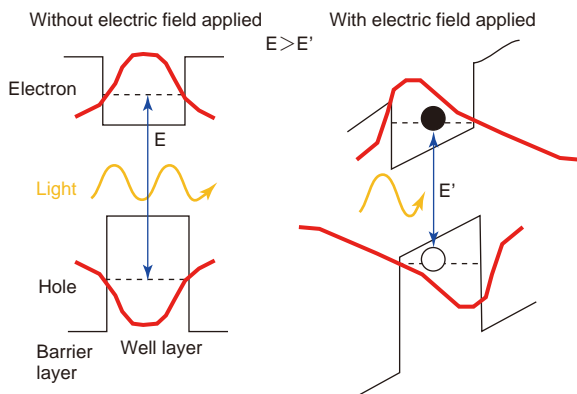


Fig. 2 Quantum confined Stark effect

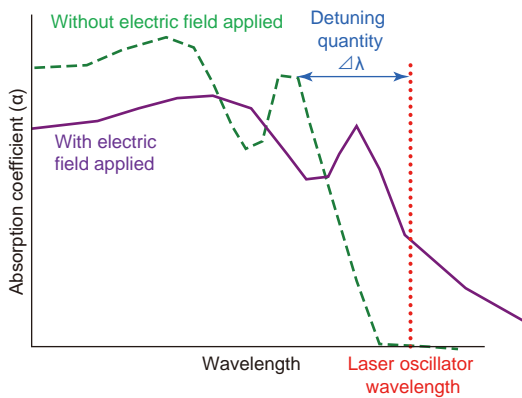


Fig. 3 Qualitative diagram of absorption spectra

through with almost no absorption; but, when an electric field is applied, the light's absorption spectrum shifts to the long wavelength side due to the quantum confined stark effect, the absorption coefficient for the laser oscillator wavelength increases, and so the light is absorbed. The electro-absorption modulator's characteristics vary widely depending on the first peak (the exciton absorption peak) of the absorption spectrum in the absence of an electric field and on the laser oscillator wavelength detuning quantity (hereinafter, referred to as " $\Delta\lambda$ "). In the normal range, the smaller $\Delta\lambda$, the greater the extinction ratio and the lower the optical output, and the larger $\Delta\lambda$, the smaller the extinction ratio and the higher the optical output. To attain the desired characteristics across a broad temperature range, it is necessary to set this $\Delta\lambda$ appropriately, but it is difficult to achieve the characteristics across a wide temperature range because the laser oscillator wavelength changes by around 0.1 nm/°C in response to the Electro-Absorption spectrum changing by around 0.5 nm/°C. At the low temperature side, $\Delta\lambda$ becomes large, so it is necessary to increase the voltage applied to attain the desired extinction ratio, but if a large voltage is applied, there is the issue that the exciton absorption peak collapses and the extinction ratio is reduced. Here, these issues are resolved by devising the absorption layer's multiple quantum well design and designing $\Delta\lambda$ appropriately. At the high temperature side, there is the issue that the laser's optical output is reduced, but even when operating at a high temperature of 85°C by devising a current blocking layer structure, we have ensured that the desired optical output can be attained.

3. EML Evaluation Result

Table 1 shows EML's target specification and evaluation results. Figure 4 shows the frequency response characteristics (S21) of the product developed here (1311 nm wavelength band chip). The measurements were made by contacting an Radio Frequency (RF) probe directly with the submount on which the chip was implemented. The operating conditions are: chip temperature $T_{LD} = 5^\circ\text{C}$, LD current (I_{op}) =

Table 1 Product target specification and evaluation results

| Item | | Target specification | Evaluation result | |
|---|----|----------------------|-------------------|------------|
| | | | 5°C | 85°C |
| Emission wavelength | L0 | 1264.5~1277.5nm | 1267.5nm | 1274.4nm |
| | L1 | 1284.5~1297.5nm | 1287.4nm | 1294.6nm |
| | L2 | 1304.5~1317.5nm | 1307.5nm | 1314.6nm |
| | L3 | 1324.5~1337.5nm | 1327.4nm | 1334.4nm |
| 3dB cutoff frequency | | $\geq 35\text{GHz}$ | 53GHz | 48GHz |
| Optical modulation amplitude (chip facet) | | $\geq 5\text{dBm}$ | 8.0~8.6dBm | 5.3~7.6dBm |
| Extinction ratio | | $\geq 3.5\text{dB}$ | 4.7~5.3dB | 7.0~7.3dB |
| TDECQ | | $\geq 3.4\text{dB}$ | 2.4~2.7dB | 1.4~2.5dB |

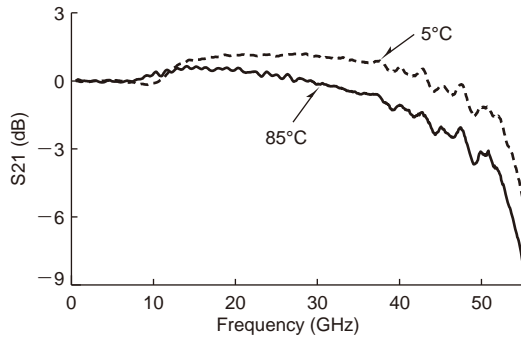


Fig. 4 Experimental result of frequency response

40 mA, EA offset voltage (V_{EA}) = -2.5 V, T_{LD} = 85°C, I_{op} = 120 mA, V_{EA} = -1.5 V. To operate the device at 100 Gbps, a passband of 35 GHz or more is required in general, and the product developed here attains a sufficient bandwidth for 100 Gbps transmission, with 53 GHz at 5°C and 48 GHz at 85°C.

Figure 5 shows the optical waveform during Back-To-Back (BTB) 53.125 Gbaud Pulse Amplitude Modulation -4 (PAM4) modulation operation for each wavelength band at chip temperatures of 5°C and 85°C. The measurements were made by contacting an RF probe directly with the submount on which the chip was implemented. The operating conditions are: baud rate of 53.125 Gbaud, EML modulation voltage amplitude (V_{pp}) of 1.0 V, I_{op} = 30 mA @ 5°C and 120 mA @ 85°C. The EA center bias

(V_c) is as shown in the respective diagrams. In the chip end output, we attained an Optical Modulation Amplitude (OMA) of 8.0 - 8.6 dBm @ 5°C, and of 5.3 - 7.6 dBm @ 85°C, an extinction ratio during modulation (Ex) of 4.7 - 5.3 dB @ 5°C, 7.0 - 7.3 dB @ 85°C, TDECQ 2.4 - 2.7 dB @ 5°C, and 1.4 - 2.5 dB @ 85°C, and so we achieved the target specification with a broad temperature range with a chip temperature of 5°C and 85°C.

4. Conclusion

We developed a CWDM 4-wavelength 100 Gbps EML chip operating at chip temperatures from 5 to 85°C, and we attained excellent characteristics that satisfied the target specification. Due to this, the optical transceiver, which is a system component in data centers, does not require a Thermo Electric Cooler (TEC) for temperature adjustment of the EML, though it was required with previous products, and can reduce the power consumption and cost in data centers.

References

- (1) 100G Lambda MSA <https://100glambda.com/>
- (2) Morita, Y., et al.: 1.3 μm 28 Gb/s EMLs with Hybrid Waveguide Structure for Low-Power-Consumption CFP2 Transceivers, Optical Fiber Communication Conference/National Fiber Optic Engineers Conference 2013, America, paper OTh4H.5 (2013)

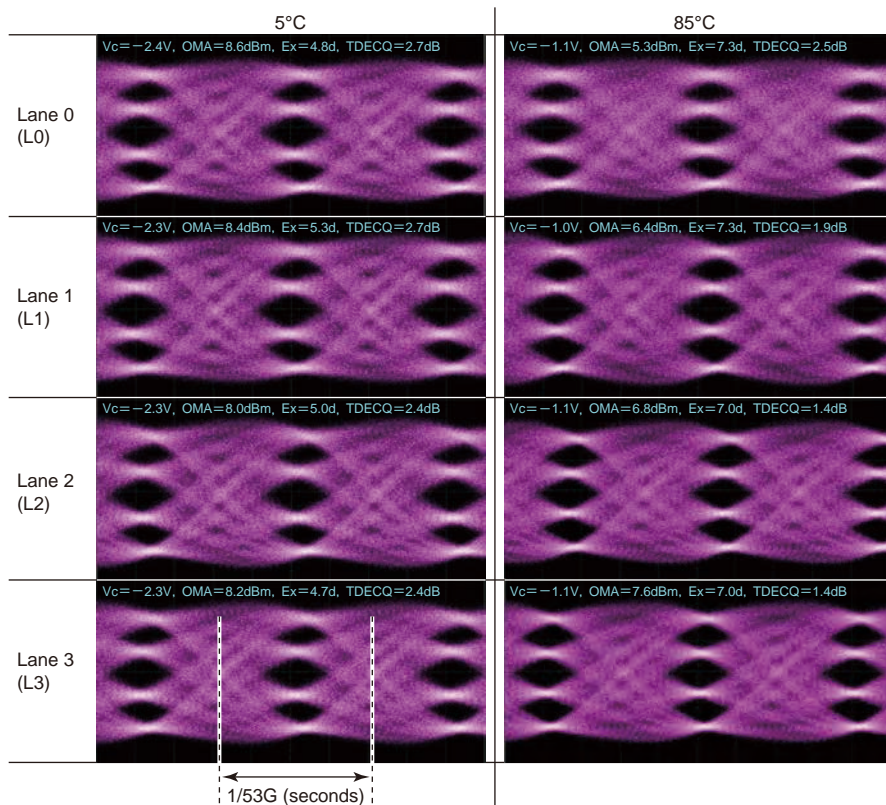


Fig. 5 53.125 Gbaud PAM4 eye diagrams

50Gbps DFB Laser Diode for 5G Base Stations

Authors: *Go Sakaino** and *Masaaki Shimada**

1. Introduction

Migration to 5G is accelerating as the volume of data communication in mobile communications is increasing. Optical communication devices used in the fronthaul antenna base stations of 5G mobile communication networks are required to operate across a broad temperature range because they are installed outdoors. In addition, a Distributed Feedback (DFB) laser is used enabling direct modulation so that low power consumption operation is achieved without the need for a thermoelectric conversion element. In the 50GBASE-LR standard supported by the fronthaul, the Pulse Amplitude Modulation -4 (PAM4) modulation method in which the light intensity is changed from the conventional two-valued to four-valued is proposed. With this modulation method, even though the DFB laser's modulation speed is the same 25 Gbps as for conventional modulation, 50 Gbps transmission is possible. Here, we designed and developed a 50 Gbps DFB laser chip and industry-standard TO-56CAN package suitable for the PAM4 modulation method.

2. Device Design

Until now, we have productized a DFB laser operating at 25 Gbps in a temperature range from -40°C to 90°C . With a direct modulation operation DFB laser, it is important to suppress the optical modulation waveform degradation due to the oscillation of the light intensity occurring as a result of the interaction of the electricity and the light. The frequency of this light intensity oscillation is referred to as the relaxation oscillation frequency and it is required to maintain a high value of the same order as the modulation frequency in the full temperature range of operation. For this reason, there is a remarkable loss of light and reduction in efficiency in injecting electric current into the active region at high temperatures in particular, and it is necessary to suppress the reduction in the light density in the active region. In addition, in a package equipped with a DFB laser chip, it is important to optimize the impedance in the design of the transmission line of the high frequency electrical signal to suppress the degradation of the high frequency characteristics.

In the use of 50GBASE-LR, the four-valued electrical

signal which changes at 26.56 Gbaud is input into the DFB laser, and the DFB laser chip outputs the four-valued light signal. The index that determines whether this optical modulation waveform is good or not is stipulated in IEEE 802.3cd, and uses the Transmitter and Dispersion Eye Closure Quaternary (TDECQ) calculated from the optical modulation waveform with the waveform shaped by the Low Pass Filter (LPF) and Feed Forward Equalizer (FFE).

Because there is a four-valued signal in the PAM4 signal waveform, the eye opening is extremely small, so there is a tendency for the waveform quality to be reduced remarkably due to the effect of the DFB laser's relaxation oscillation. We conducted a simulation using a model based on the DFB chip model which takes into consideration this relaxation oscillation and the 25 Gbps DFB laser's package developed in 2018, and designed the DFB laser chip and package. The results are shown in Fig. 1.

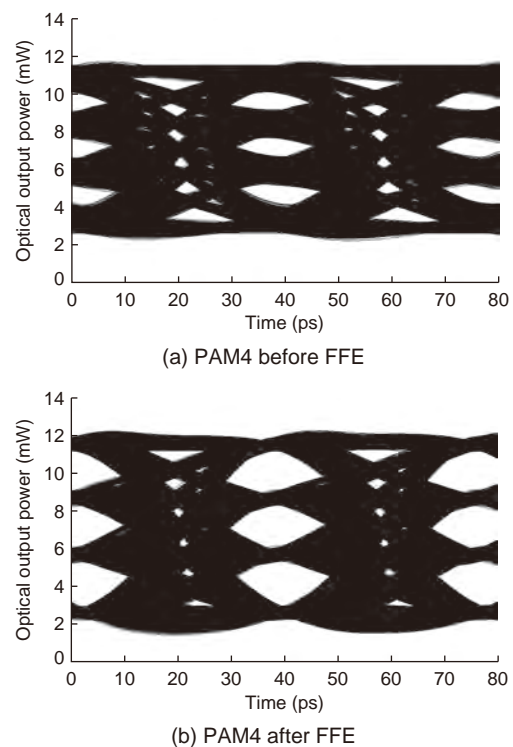


Fig. 1 Simulated waveforms

3. Device Structure and Characteristics

Figure 2 shows an outline photograph of the 50 Gbps DFB laser with an oscillating wavelength of 1310 nm developed here. The outline of the CAN package uses the industry-standard Φ 5.6 mm TO-CAN which makes it possible to secure compatibility with the previous product and to conform with the compact transceiver standard (SFP56).



Fig. 2 50Gbps DFB laser

The electric current and optical output characteristics are shown in Fig. 3. In the operating temperature range from a low temperature of -40°C to a high temperature of 90°C , the threshold current and the change in the slope efficiency are small, so we were able to achieve sufficient characteristics for 50GBASE-LR. At the high temperature of 90°C in particular, we achieved a threshold current of 20 mA or less, a slope efficiency of 0.22 mW/mA or more, and a maximum optical output of 12 mW or more.

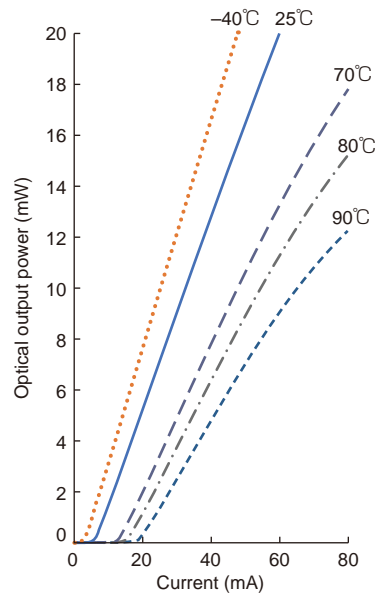


Fig. 3 I - L characteristics ($-40, 25, 70, 80, 90^{\circ}\text{C}$)

Figure 4 shows the PAM4 transmission optical modulation waveform. The optical waveform is observed after applying the LPF and the FFE, and the TDECQ was calculated using a method conforming to IEEE 802.3cd. In addition, in order to correct the DFB laser's frequency response, the Pre-Emphasis which highlights the electrical signal's rising edge and falling edge in advance is used and the TDECQ can be improved. In recent years, driver ICs have been put into use with improved PE performance, and here, we also conducted a comparison with and without the PE applied. From the low temperature to the high temperature, whether the PE is applied or not, a large eye opening is achieved and, even after 20 km transmission, the optical modulation waveform is excellent with little disturbance.

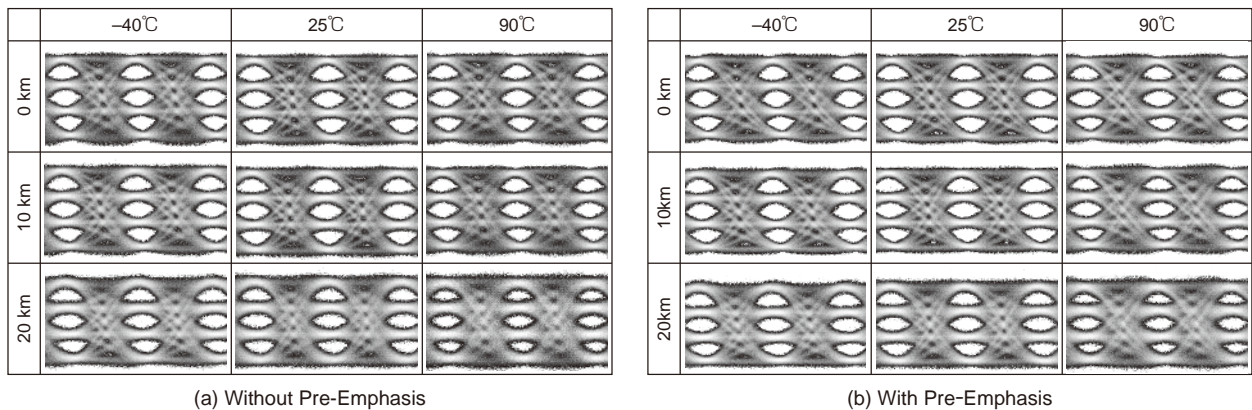
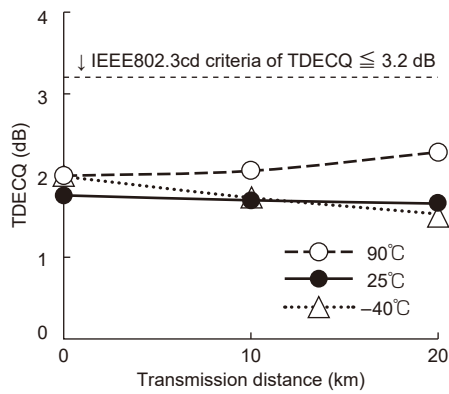
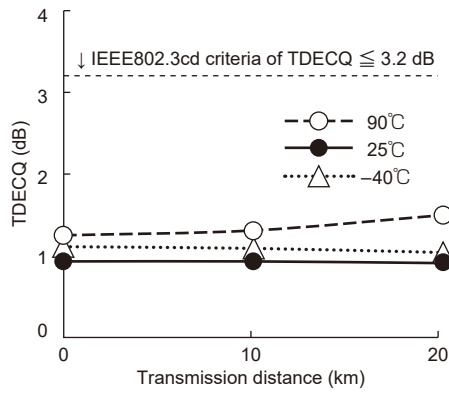


Fig. 4 Optical waveforms after transmission

Figure 5 shows the TDECQ transmission distance dependency. The TDECQ with no PE applied at temperatures of -40°C , 25°C , and 90°C are 2.3 dB, 1.8 dB, and 2.0 dB respectively before transmission (0 km). Furthermore, during the 10 km transmission required of 50GBASE-LR, the values are 2.1 dB, 1.7 dB, and 2.1 dB, which sufficiently satisfy the standard of 3.2 dB or less. In addition, when the PE is applied, the TDECQ after the 10 km transmission are 1.1 dB, 0.9 dB, and 1.3 dB, so that the effect of applying the PE is confirmed.



(a) Without Pre-Emphasis



(b) With Pre-Emphasis

Fig. 5 Dependence of TDECQ on transmission distance

4. Conclusion

We developed a 50 Gbps DFB laser suitable for the PAM4 modulation method targeting the fronthaul of 5G mobile communication networks. Characteristics satisfying the standard 50GBASE-LR standard were achieved, the speed was doubled compared to the previous device to this one, and we were able to realize 5G high speeds and low power consumption.

References

- (1) IEEE Standards Association : IEEE 802.3cd 50Gb/s, 100Gb/s and 200Gb/s Ethernet Task Force <https://www.ieee802.org/3/cd/>
- (2) Sakaino, G., et al.: Direct Modulation DFB Laser for 25 Gbps Optical Transmission, Mitsubishi Electric ADVANCE Mar.2018 Vol.161, 2~4 (2018)

1.55 μm Tunable DFB-LD for 400G Digital Coherent Optical Transmission System

Authors: Kazuki Yamaji* and Ryosuke Nagao*

1. Introduction

In metro and long-haul networks, data center interconnects, and so on, the demand is rising for high speed, large capacity digital coherent communication.

In this article, we describe the development of a wideband, tunable Distributed Feedback Laser Diode (DFB-LD) chip targeting 400 Gbps digital coherent communication with integrated 16-array DFB-LD and Semiconductor Optical Amplifier (SOA).

2. Background

Because the speed and capacity of optical communication devices are increasing as communication traffic increases, multi-value modulation and light polarization are used, and the demand is rising⁽¹⁾ for digital coherent communication using digital signal processing in modulation and demodulation, so wideband variable wavelength lasers are required as local light sources for that signal beam and the optical receiver. In recent years in particular, the demand has been rising for a speed increase from the conventional 100 Gbps to 400 Gbps in metro and long-haul networks and data center interconnects.

400G digital coherent communication employs 16QAM (Quadrature Amplitude Modulation) or 64QAM, which are the combination of intensity modulation of the optical spectrum and QPSK (Quadrature Phase-Shift Keying) which modulates optical signals by changing the light's phase shift. Such modulation methods require a light source with low phase noise, narrow spectral linewidth, and sufficient intensity. The industry standards group, the Optical Networking Forum (ONF), proposes the specification for the light sources such as Micro-Integrable Tunable Laser Assembly (ITLA), etc. applied to those modulation methods. The specification also includes other requirements such as wavelength grid, wavelength stability, etc.

The wavelength-tunable laser methods include the external resonator type, the Distributed Bragg Reflector (DBR) type, and the Distributed Feedback (DFB) array type as shown in Table 1. In the development we are describing here, we used a DFB array type which can realize stable optical output with a simple control to develop the ML9CP61 tunable DFB-LD chip with integrated SOA to supplement the light intensity.

Table 1 Tunable laser type

| Type | Output power | Optical spectral linewidth | Tunable range of wavelength | Controllability |
|--------------------|--------------|----------------------------|-----------------------------|-----------------|
| External resonator | △ | ○ | △ | △ |
| DBR | ○ | △ | ○ | × |
| DFB array | △ | △ | ○ | ○ |

3. Tunable DFB-LD Chip Design

Figure 1 shows the structure of the tunable DFB-LD chip we developed. Integrated into the InP substrate are 16 DFB-LDs with differing oscillating wavelengths, 16 x 1 Multi Mode Interferer (MMI) optical couplers combining the DFB-LD's optical output in the output port, and SOA to compensate for the losses occurring in the optical couplers and to amplify the optical output. For the purpose of a reduction in the reflected return light, the SOA waveguide is inclined and, at the same time, the chip end surface has a window structure with anti-reflective coating. The chip size is 3.8 mm x 0.75 mm x 0.1 mm.

Changes in the oscillating wavelengths are carried out through the selection of the DFB-LD and the chip temperature adjustment using the Thermoelectric Cooler (TEC). Because the temperature dependency of DFB-LD oscillating wavelength is small at approximately 0.1 nm/°C, in the case that DFB-LD array number is small, it is necessary to significantly change the chip temperature, so the TEC's power consumption is

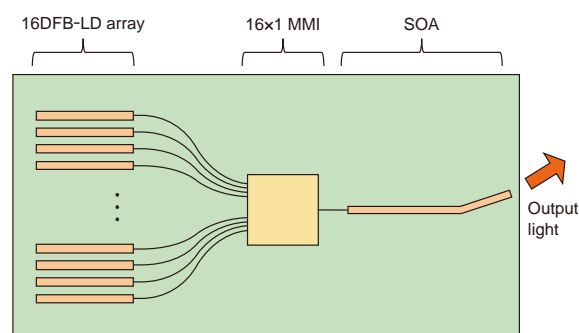


Fig. 1 Schematic structure of tunable DFB-LD chip

increased. When there are many arrays, although the losses in the optical coupler parts increase, it is possible to narrow the temperature adjustment range and this is advantageous for reducing the power consumption. Here, the number of arrays is 16 and the temperature range is 25 - 55°C, and the diffraction grating pitch of each DFB-LD is designed to satisfy the wavelength standard of the 1.55 μm band of OIF-IC-TROSA-01.0⁽³⁾ and OIF-400ZR-01.0⁽⁴⁾. To realize the light spectral linewidth of 500 kHz or less required for digital coherent communication, the diffraction grating length was lengthened to 1.4 mm.

4. Element Characteristics

Figure 2 shows the optical output power of the fabricated tunable DFB-LD chip. The Laser Diode (LD) current was set to 220 mA (chip temperature of 25°C) or 250 mA (chip temperature of 55°C), and the SOA current was set to 400 mA. It was confirmed that an optical output of 17 dBm or more was obtained with a variation of 1 dB or less across the full range of the 1.55 μm band. Figure 3 shows the output light spectrum when one of the DFB-LD arrays is operated. The tunable wavelength width corresponding to one DFB-LD at a chip temperature from 25°C to 55°C is 2.9 nm. The Side Mode Suppression

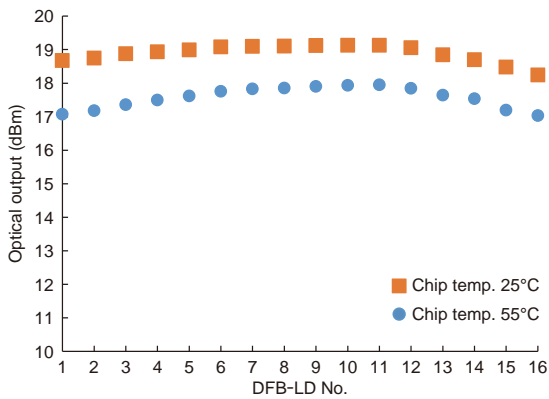


Fig. 2 Output light power of tunable DFB-LD chip

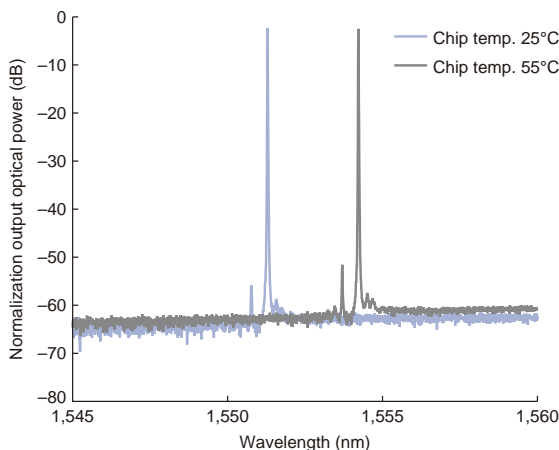


Fig. 3 Optical spectrum of a DFB-LD output light

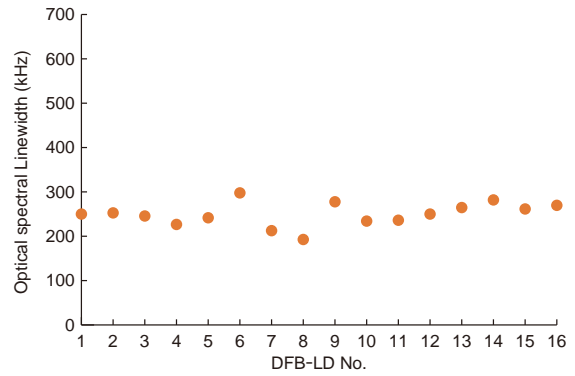


Fig. 4 Optical spectral linewidth of tunable DFB-LD chip

Ratio (SMSR) maintains 45 dB or more in an operating temperature range of 25°C to 55°C.

Figure 4 shows the light spectral linewidths at 55°C, an LD current of 250 mA, and an SOA current of 400 mA. The light spectral linewidths are 300 kHz or less, so realization of the performance target of 500 kHz or less was confirmed.

5. LD Modularization

The LD module in Fig. 5 was prototyped using the fabricated DFB-LD chip. Figure 6 shows the block diagram. The output light of the DFB-LD chip parallelized with a collimating lens is separated by prisms 1 and 2, then input respectively into a light intensity monitor PhotoDiode (PD) and a PD for use with a wavelength

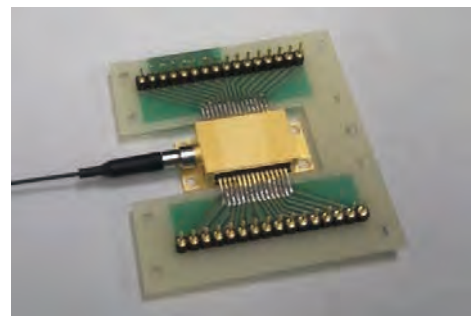


Fig. 5 LD module

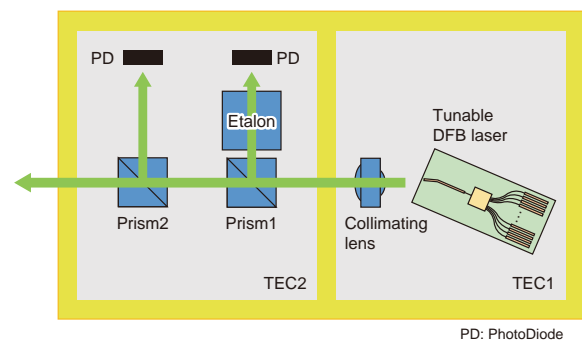


Fig. 6 Schematic block diagram of LD module

monitor via an etalon. To control the temperature independently of the DFB-LD chip, the DFB-LD chip and the collimating lens are installed above TEC1, and the other parts are installed above TEC2.

Figure 7 shows the LD module's tunable wavelength range. The drive current was supplied to the 16 DFB-LDs in order, the chip temperature was kept between 25°C and 55°C, and the oscillating wavelength was measured. It was confirmed that the tunable wavelength range was from 1526.49 nm to 1567.94 nm and that the OIF-IC-TROSA-01.0 (1527.99 nm - 1566.72 nm) and the OIF-400ZR-01.0 (1528.77 nm - 1567.13 nm) were satisfied.

Figure 8 shows the power consumption simulation results and the evaluation results. The total values of the power consumption of the LD chip and the TEC are shown in the case that the LD module temperature was changed to between -5°C and 75°C while keeping the temperature of the LD chip on TEC1 to 25°C or 55°C. In the simulation, the maximum was 4.0 W with an LD chip temperature of 25°C and an LD module temperature of 75°C. The measurement result was 4.3 W under the same conditions so a value close to the designed one was obtained, and meeting the power consumption specifications of the OIF MicroITLA was estimated to be possible.

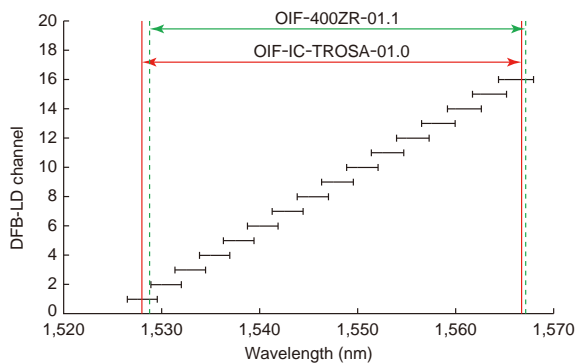


Fig. 7 Tunable range of oscillation wavelength of LD module with DFB-LD chip temperature controlled in the range of 25°C to 55°C

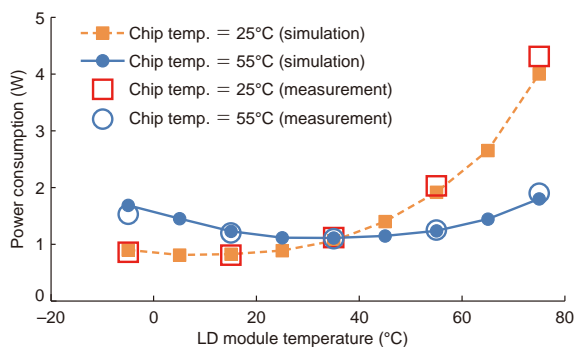


Fig. 8 Power consumption of LD module

6. Conclusion

We developed a tunable DFB-LD chip for use with 400 Gbps digital coherent communication integrated with 16 DFB-LDs with differing oscillating wavelengths and SOA. We realized characteristics suitable for 400 Gbps digital coherent communication with optical output ≥ 17 dBm, SMSR ≥ 45 dB, linewidth ≤ 300 kHz, and a wavelength range of 1526.49 nm to 1567.94 nm.

We expect that the technology developed here will contribute to increasing the capacity of digital coherent communication and contribute to an optimal package design for the customers' optical transceiver.

References

- (1) Suzuki, S., et al.: Research and Development of Digital Coherent Signal Processing Technology for Increasing the Capacity of Optical Communication Networks, Journal of the Institute of Electronic Information and Communication Engineers, 95, No. 12, 1100 - 1200 (2012)
- (2) OIF-MicroITLA-01.1
<https://www.oiforum.com/wp-content/uploads/2019/01/OIF-Micro-ITLA-01.1.pdf>
- (3) OIF-IC-TROSA-01.0
<https://www.oiforum.com/wp-content/uploads/OIF-IC-TROSA-01.0.pdf>
- (4) OIF-400ZR-01.0
https://www.oiforum.com/wp-content/uploads/OIF-400ZR-01.0_reduced2.pdf

Thermal Diode Infrared Sensor “MelDIR” and User Support Tools

Authors: Yasuki Aihara* and Satoshi Okuda*

1. Introduction

IoT is essential in our lives and accompanying this we are surrounded by a variety of sensors. Among those are infrared sensors whose characteristics include the ability to detect people and objects while securing privacy. In this paper, we introduce the features of the thermal diode infrared sensor MelDIR which uses Mitsubishi Electric unique technology and we introduce the development of user support tools which support customers from product planning to commercialization.

2. Thermal Diode Infrared Sensor

The infrared sensor has a function which detects and enables visualization of the heat from objects without contact by converting the infrared radiation received into an electric signal. Figure 1 shows those features. (1) Because the sensor can acquire the heat information from the heat source without contact, it is excellent from the view of hygiene and safety. (2) It can determine a person's motion or posture from the silhouette of the heat source. This is particularly effective in scenarios where privacy protection is required, so the sensor can be used even in toilets or bathrooms where cameras

cannot be installed. (3) The heat source can be detected even in darkness or where there is no visibility due to smoke, so the sensor can be used with peace of mind even indoors at night.

Mitsubishi Electric developed new resolution and price range product MelDIR compared to conventional thermopiles and bolometers using its unique thermal diode sensor technology.

The thermal diode Technology features the use of a PN junction diode formed in the general silicon semiconductor manufacturing process for the temperature detection area. This technology has good compatibility with semiconductor processes as well as for bolometers, so it's suitable for multi-pixelization. The thermal diode performs thermoelectric conversion by detecting the temperature dependence of the forward voltage drop of the diode.

The forward voltage of the diode changes approximately linearly with temperature, and its characteristics are determined by the process conditions of the semiconductor, so it can be manufactured with high uniformity.

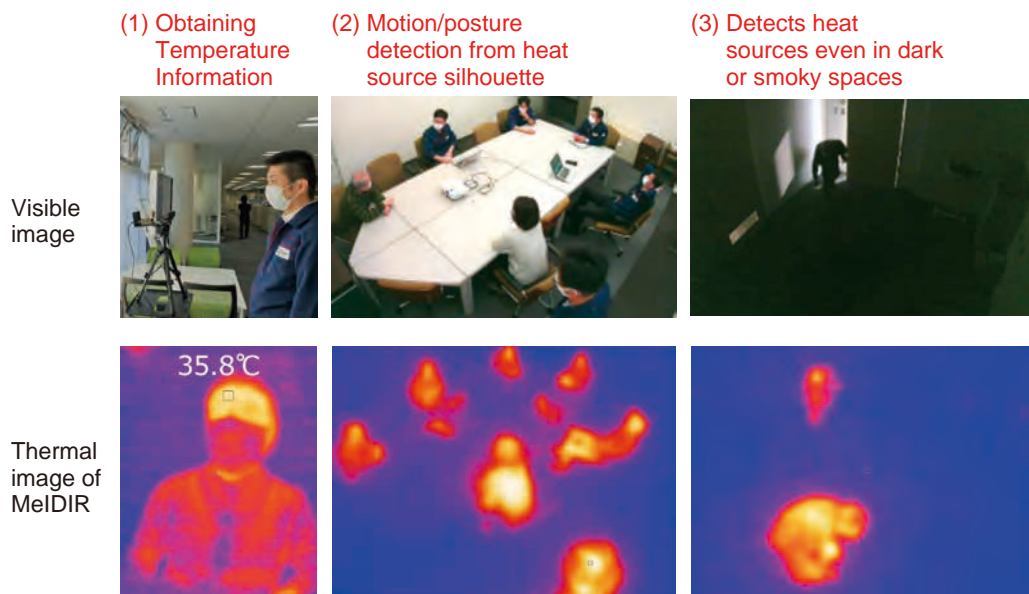


Fig. 1 Features of infrared sensor

3. MeIDIR Thermal Diode Infrared Sensor

The conventional infrared sensor market has polarized into low pixel, low cost products for heat detection uses, and high pixel, high price infrared cameras for infrared imaging uses. Using unique technology, Mitsubishi Electric developed infrared sensor module MeIDIR with a high pixel count at an unprecedented low cost. Table 1 shows our product lineup. In 2019, we released the MIR8032B1, and it was used mainly in Japan for monitoring in elderly people's facilities and was also installed in air conditioners. In 2023, we released the MIR8060B3, targeting markets such as factory equipment surveillance and kitchen temperature management which require object detection at higher temperatures. This product increased the maximum measurable object temperature from +60°C to +200°C by optimizing the signal processing and the lens.

Because the thermal infrared sensor thermoelectrically converts the temperature rise part, the detection sensitivity falls if the heat conductance is high between the temperature detection area and the surrounding environment. In addition, if the heat conductance is high between the surrounding pixels, the resolution decreases because the heat detected by the pixels is transmitted to the surrounding pixels. Therefore, the space between the diode and the silicon substrate is hollowed out to form a structure in which the diode is held by supporting legs. By placing the electric line in these support legs, the thermal conductance between the diode and the silicon substrate is lowered while maintaining the structure and electrical connection. This supporting leg structure is formed by carrying out dry etching of the thin film Silicon On Insulator (SOI) substrate which enables low cost manufacture. Figure 2 shows a SEM image of thermal diode area. It can be confirmed that the hollowed out structure, in which the 25 μm pitch temperature detection area is maintained by the supporting leg structure, is

formed uniformly.

4. User Support Tools

Figure 3 shows the series of user support tools. We have prepared a proposal paper to support the customer's product concept making stage. It provides a wealth of thermal image examples to show them ideas of how to use MeIDIR, it indicates the benefits, etc. of adopting MeIDIR, and provides a stepping stone for starting their evaluation.

We provide a dedicated demo kit for customers to evaluate MeIDIR. In 2022, We released the EVA series of demo kits, that integrate MeIDIR, shutters, and substrates and further reduce the substrate area to about 45% of the conventional size. Figure 4 shows a photograph of the demo kit. It's available and ready to use, it does not require any additional time for evaluation preparation.

In order to provide design information for the required hardware and software at the customer's product development stage, we developed a reference design. The reference design summarizes the design information of the EVA series demo kit, and the design information for hardware such as BOM and Gerber, and

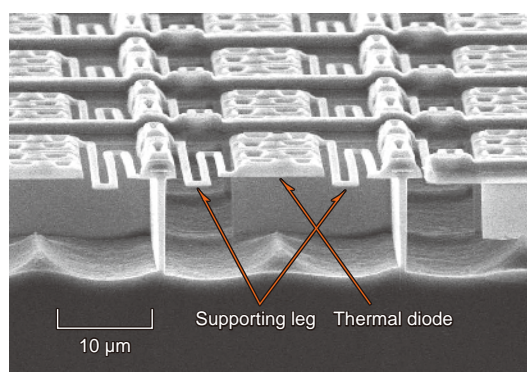
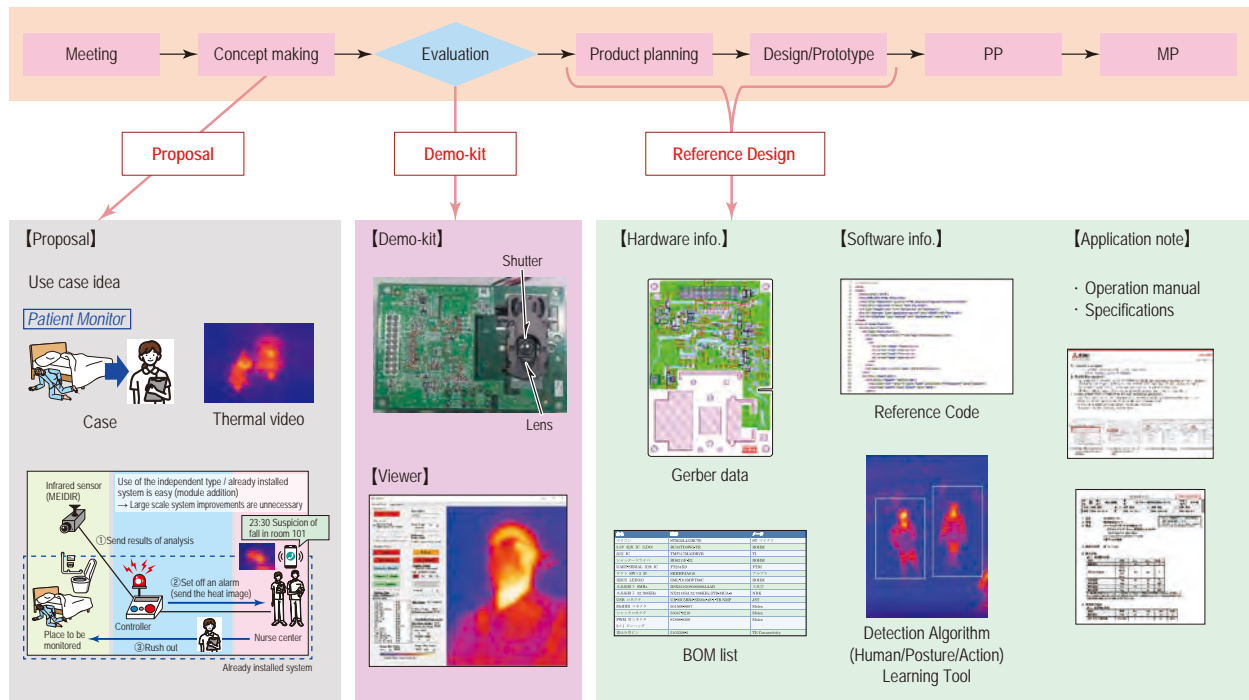


Fig. 2 SEM image of thermal diode

Table 1 MeIDIR product lineup

| Type No. | MIR8060B3 | MIR8060B1 | MIR8032B1 |
|------------------------------|-----------------------------------|-------------------------|-------------------|
| Launch date | Mar. 2023 | Jul. 2021 | Nov. 2019 |
| Detectable temperature range | -5°C ~ +200°C | -5°C ~ +60°C | -5°C ~ +60°C |
| Number of Pixels | 80×60 | 80×60 | 80×32 |
| Field of View | 78°×53° (Typ.) | 78°×53° (Typ.) | 78°×29° (Typ.) |
| Frame Rate | 4 / 8 fps Selectable | 4 / 8 fps Selectable | 4 fps Fixed |
| NETD | 250 mK (Typ.) | 100 mK (Typ.) | 100 mK (Typ.) |
| Power consumption | 50 mA or less | | |
| Module Size | 19.5×13.5×9.5 mm | | |
| Communication interface | Serial Peripheral Interface (SPI) | | |



All stage in development would be supported by each tool

Fig. 3 MeDIR User Support Tools



Fig. 4 Demo kit "EVA-MIR8060B1-MC02V1-01"

Table 2 Heat source detection algorithm and hardware specifications

| Item | Specification |
|----------------------------|---|
| Type No. | MIR8060B1-01 |
| Type No. of Demo kit | EVB-8060B1-MN**** |
| Type No. of reference code | SAPM-MD**V** |
| Target MCU | STM32H723_G (Cortex-M7 1177 DMIPS@530MHz) |
| Deep learning algorithm | MobileNetV2-YOLOv3-Nano |
| Rom size | <1Mbyte |
| Ram size | <512Kbyte |
| Frame rate | 7fps(=142ms/frame) |

the software design such as object detection by deep learning and reference code, and application notes such as several kind of manuals. These tools contribute to reducing product development period.

We provide heat source detection algorithm using the deep learning in reference designs. The detection algorithm based on You Only Look Once (YOLO) is optimized for use with MeDIR, and it has the characteristic that it is developed as an edge AI to target a general-purpose Micro Controller Unit (MCU) for embedded use. Table 2 shows the heat source detection algorithm and the hardware specifications.

Since November 2022, we have been offering two

algorithms: a human detection algorithm which detects people in a living room, and a posture detection algorithm which detects the posture in a toilet stall and judges whether or not there is any abnormality.

The detection algorithms provided may not achieve sufficient detection accuracy depending on the customer's usage conditions. For this reason, we developed and have been offering a model training tool (MTT-V001) with the purpose of creating an AI model to match the respective usage environments. Furthermore, we have been also offering a manual to summarize the series of work procedures of extraction of gray scale images, annotations, AI model creation, and embedding

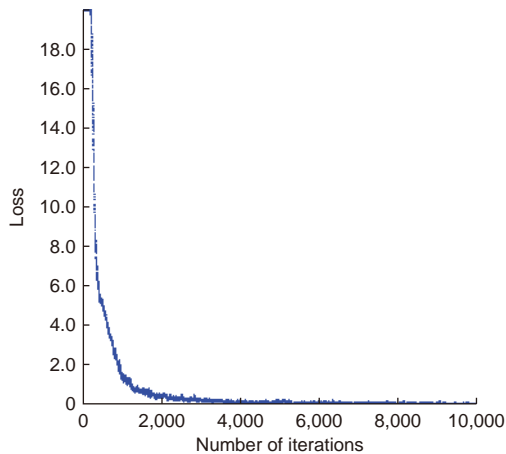


Fig. 5 Example of a training result

in a MCU, and are arranging an environment in which the customer themselves can optimize for their own products.

Figure 5 shows an example of the training result. It shows that as the number of iterations increases, the loss is decreased and the calculation is converged. In this example, for 10,000 iterations, mean Average Precision (mAP), which is the detection rate index, achieves 80% or more.

5. Conclusion

We released MIR8060B3 as a new product of MelDIR in 2023. By expanding the upper limit of the detection temperature range from the conventional +60°C to +200°C, we have made it possible to meet the growing needs of monitoring factory equipment and temperature control in kitchens. Furthermore, we have enhanced our user support tools to assist in customer evaluation and product development, contributing to a reduction in time to market. We released the EVA series of demo kits, that integrate MelDIR, shutters, and substrates and further reduce the substrate area to about 45% of the conventional size. Furthermore, in order to provide the hardware and software design information necessary for the customer's product development, we prepared a reference design.

We aim to expand the application of these product lineup and support tools to a wide variety of fields, and contribute to the realization of secure, safe, and healthy society.

